Stationary waves in a nonlinear periodic medium: Strong resonances and localized structures. I. The discrete model

J. Coste and J. Peyraud
Laboratoire de Physique de la Matière Condensée, Université de Nice, Parc Valrose, 06034 Nice CEDEX, France
(Received 18 March 1988; revised manuscript received 6 March 1989)

The stationary-wave equation in a periodic, nonlinear medium is studied as a nonintegrable dynamical system. Two main properties are shown: (i) There exist four types of "localized solutions" which correspond to the four strong resonances of the dynamical system, one of which is the so-called "gap soliton" already described by Mills and Trullinger [Phys. Rev. B **36**, 947 (1987)]. (ii) These solutions are close to analytic ones; however, they are weakly chaotic, and this stochasticity is responsible for observable physical effects. In particular, it assigns a maximum spatial extension to the localized structures. Near the bifurcation giving rise to a localized solution, the onset of stochasticity is shown to be a critical phenomenon, whose critical exponent is evaluated. In this paper we consider a discrete model. In the following paper, we consider a continuous model.

I. INTRODUCTION

The propagation of a wave in a periodic nonlinear medium is a new, interesting problem. Up to now, only stationary waves have been considered, and from two different points of view: (i) Delyon *et al.*[1] have shown that the transmission of a wave through a finite sample exhibits nonanalytic properties, and (ii) Mills and Trullinger[2] have described analytical solutions in the first gap of the linearized system, the so-called "gap solitons."

These two aspects of the propagation look antinomic. Actually they are not. Indeed the stationary-wave equation is a nonintegrable dynamical system, and its solutions are generically nonanalytic. The phenomena described by Delyon *et al.* occur at finite wave amplitude: then the stochastic behavior of the solutions is immediately perceptible. On the other hand, the gap solitons are only weakly chaotic.

We shall be primarily interested, in this paper, in stationary waves which are close (in an appropriate sense) to analytic and localized solutions of the wave equation. By "localized" we loosely mean that some physical attribute of the wave (amplitude, phase, or eventually polarization) exhibits a rapid variation around some space points. Gap solitons belong to this class, but we shall see other types. The analysis of these structures is considerably clarified if the dynamical system is described as a mapping of the plane into itself, and this will be realized in the two models which we propose to consider. In these models the nonlinearity is cubic and, in the case of light propagation, it would be produced by the auto-Kerr effect. In the "discrete model" the propagation constant (the refractive index in the light problem) exhibits sudden jumps on equidistant sites. Then the mapping takes the form

$$F:\ (\Phi_n,\Phi_{n+1})\rightarrow(\Phi_{n+1},\Phi_{n+2})\ ,$$

Φ_n being the wave amplitude on the nth site (which will prove to be real in the present problem). In the "continuous model" the refractive index is harmonically modulated, and one defines a Poincaré map G of the continuous flow:

$$G:\ (\Phi,d\Phi/dx)_x\rightarrow(\Phi,d\Phi/dx)_{x+L}\ ,$$

where $\Phi(x)$ is the continuous wave amplitude and L is the period of the modulation externally imposed to the medium.

Now the central point is the following. Let P be an elliptic fixed point of the mapping (or if one of its iterates). When the winding number ν of P, which is a continuous function of the system control parameters, takes a rational value, a periodic cycle bifurcates at P with some period q, and the elliptic points of this cycle are created with zero winding number. As a result, mapping $F^{(q)}$ can be approximated by a first-order differential equation and the dynamical system becomes integrable. Actually this property is consistent with the Kol'mogorov-Arnol'd-Moser (KAM) theorem which says that regular closed orbits are expected in an open neighborhood of P. However, some bifurcations are "more beautiful" (or dangerous) than the others: these are the so-called "strong or Arnol'd resonances" which appear when $\nu=1/n$, with $n=1,2,3,4$. Then the KAM orbits around P are strongly perturbed and, as a result, localized solutions appear. The two first resonances occur either in the gaps *(gap solitons)* or in their neighborhood, giving *kinklike* solutions (in the terminology of optics they would be called "dark solitons"). The third and fourth resonances appear either in the gaps or in the passing bands, giving rise to new structures which we call "triangles" and "squares."

Let us now come back to the chaotic behavior of the localized solutions. A first observation is that these solutions are "small-amplitude" ones (i.e., the wave parameters exhibit small amplitude variations around isolated space points). Indeed, perfect localization is only obtained at resonance value, where the amplitude vanishes; the system is then exactly integrable. One could expect

that weak stochasticity would produce only small observable effects. That is untrue. In particular, we show that stochasticity imposes a maximum spatial extent (MSE) to a localized structure. This means that, in contradistinction to the case of an integrable system, a large propagative medium cannot support a one-peak localized solution: only multipeaks solutions are available. Moreover, numerical investigation suggests that MSE exhibits a critical behavior near a bifurcation value: it diverges as $\lambda^{-\nu}$, λ being the deviation of the wave number from its bifurcation value and ν a universal critical exponent. We evaluate ν in the two models and find indeed the same value.

Our work is presented in two successive papers. In the present one (paper I) we analyze the discrete model. This model has several advantages. First, it is already classified among the admitted nonintegrable dynamical systems (see, for instance, Gumowski and Mira[3]), and it is simpler than the continuous model, in the sense that we do not have to deal with a Poincaré map. We also note an interesting property from the experimental point of view: the gaps of the linearized system have all equal size, which makes it possible to observe localized structures at high Bragg order.

In the second paper (paper II) we study more briefly the continuous model which introduces some new features, and also removes some unphysical aspects of the first model such as the dissymmetry of the solutions versus the sign of the Kerr constant. We also include a general discussion of the physical observability of the stationary localized structures.

II. THE DISCRETE MODEL

A. General considerations

We assume that refractive index $n(x)$ exhibits δ-like jumps on equidistant sites:

$$n(x)=1+\sum_m \varepsilon_m \delta(x-m) , \tag{1}$$

where

$$\varepsilon_m=\varepsilon(1+\mu|\Psi_m|^2) , \tag{2}$$

Ψ_m being the wave amplitude on the mth site, and ε the modulation amplitude parameter. This model would be realized by a set of thin nonlinear dielectric sheaths.

It is easily shown (see the Appendix) that such a model yields, through an appropriate limit, the following recursion relation obeyed by the Ψ_m's:

$$\Psi_{m+1}+\Psi_{m-1}=E_m\Psi_m \tag{3}$$

with

$$E_m=2[\cos k-\varepsilon \sin k\,(1+\mu|\Psi_m|^2)] , \tag{4}$$

where k is the wave number, and the nonlinear term would represent in optics the auto-Kerr effect. Setting $U_m=\Psi_m, V_m=\Psi_{m+1}$, relation (3) is equivalent to the mapping of the plane into itself:

$$F:\ (U_m,V_m)\rightarrow(U_{m+1},V_{m+1})$$

defined by

$$U_{m+1}=V_m ,$$
$$V_{m+1}=-U_m+E_mV_m .$$

This equation looks like a discretized version of the stationary nonlinear Schrödinger equation, and it has been recently used by Delyon, Levy, and Souillard[1] for studying the transmission of a wave in a finite periodic nonlinear medium. However, these authors use a different definition of energy parameter E_n, namely

$$E_m=2\cos k-\mu|\Psi_m|^2 . \tag{5}$$

In this expression, our parameter ε, characterizing the modulation of the refractive index in the absence of the Kerr effect, does not enter. This form of E_m also implies that the linearized system is only to be found in a passing band, actually in the first Brillouin zone. Moreover, the coefficient of the nonlinear term in expression (4) is k independent. But we show in the Appendix that this is not allowed if Eq. (3) is to represent the propagation of a wave in a stratified medium.

Equation (3) has the property of conserving the wave energy flux $J=2i(\Psi_n\Psi^*_{n+1}-\Psi^*_n\Psi_{n+1})$. Moreover, they are invariant in the change $\Psi_n\rightarrow e^{i\theta}\Psi_n$ (gauge invariance), θ being an arbitrary angle. These two properties have the following important consequences. (a) If the flux is null, then Ψ_n, solution of Eq (3), can be taken real. Indeed, $J=0$ implies that $\psi_n/\psi^*_n=\psi_{n+1}/\psi^*_{n+1}$, and therefore the phase of the complex number Ψ_n is preserved in the course of the iteration of the mapping. Then the gauge invariance permits one to take Ψ_n real. (b) Reciprocally let us consider a fixed point ξ of F. Its phase is constant and, as a result, $J(\xi)$ vanishes. Obviously these properties also pertain to any iterate $F^{(p)}$ of the mapping. Therefore any fixed point of $F^{(p)}$, that is, any periodic orbit of F with period p, cannot exist except in a zero-flux system. But we shall see in the following that the localized solutions are associated with homoclinic or heteroclinic orbits of the mapping, that is, connecting periodic points. Therefore we shall limit ourselves in this paper to the study of zero-flux systems. Of course, relaxing this restriction poses an interesting problem which obviously involves nonstationary waves (time-dependent problem). We shall show in a subsequent paper that there exist nonzero flux solutions which are localized with analogous shapes, but propagative.

Taking Ψ_n real and setting

$$\Phi_n=\Psi_n\sqrt{|2\varepsilon\mu\sin K|} , \tag{6}$$

$$X=\Phi_n \quad Y=\Phi_{n+1} , \tag{7}$$

we obtain, in the zero-flux case, the following mapping:

$$f:\ (X,Y)\rightarrow(X',Y')$$

such that

$$X'=Y , \tag{8}$$
$$Y'=-X+E_0Y-\eta Y^3 ,$$

with

$$E_0=2(\cos k-\varepsilon\sin k)\ , \tag{9}$$

$$\eta=\mathrm{sgn}(\varepsilon\mu\sin k)=\pm 1\ . \tag{10}$$

A remarkable property of the model is that μ enters the above equations only through its sign. Therefore, $|\mu|$ contributes to the solutions only as a scaling factor. We also remark that the sign of ε is not a relevant physical parameter. Indeed the mapping equations are invariant in the change ($\varepsilon\mapsto-\varepsilon$, $k\mapsto-k$). The mapping can be studied in terms of the only parameters E_0 and η; then the results will be interpreted in terms of parameter k, ε, and $\mathrm{sgn}(\mu)$ with the help of relations (9) and (10).

B. Elementary properties of the mapping: Symmetries and fixed points

The dynamical system described by Eqs. (8) belongs to a class of conservative systems already considered in the literature (see, for instance, Gumowski and Mira[3] and Bak and Pokrovsky[4]) but most of its mathematical properties are still unknown (as are those of any nonintegrable mapping of the plane into itself). However, some simple remarks can be made.

First, being given an orbit of the mapping, there exist two other orbits, respectively, symmetric from the first one versus the first and the second bissectrix. The symmetry versus the first bissectrix is readily shown by inverting the sense of light propagation through the system. The second symmetry results from the first one and from the symmetry of the mapping transformation versus the origin [the change $(X\mapsto-X, Y\mapsto-Y)$ implies $(X'\mapsto-X', Y'\mapsto-Y')$].

Second *(Symmetry property S),* when inverting the sign of the parameters ($\{E_0,\eta\}\to\{-E_0,-\eta\}$), an orbit solution $\{X_k\}$ of the first system is transformed to $\{(-1)^k X_k\}$ in the second one, and the fixed points of f are transformed to those of $f^{(2)}=f_0 f$. This allows us to restrict the study of the mapping to one value of η, say $\eta=-1$.

1. *Fixed points of f and f² bifurcation diagrams*

A first fixed point of f is the origin. It is stable (elliptic) or unstable (hyperbolic) according to whether or not

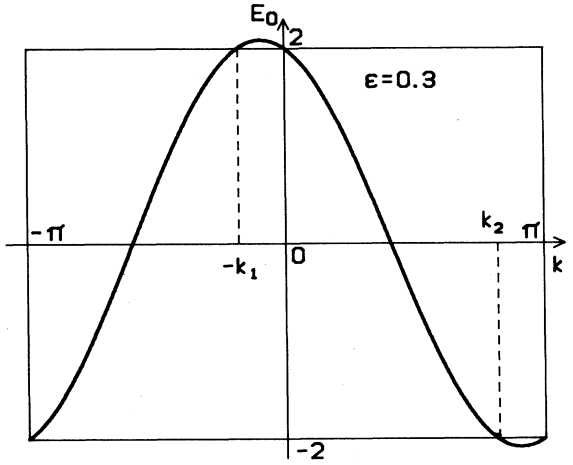

FIG. 1. Graph of $E_0(k)$ for $\varepsilon=0.3$.

E_0 belongs to interval $[-2,2]$. In other words, this interval corresponds to the passing bands (PB) of the linearized system, while gaps (or stop bands) are found outside. In a passing band, the eigenvalues of the linearized mapping at the origin are $e^{\pm i\varphi}$, where φ is given by

$$\cos\varphi=E_0/2 \tag{11}$$

and the winding number of the origin is $\nu=\varphi/(2\pi)$.

It is worth remarking that the gaps are found in finite bands of wave number k, which vanish in the limit of small ε. Figure 1 shows the graph of E_0 as a function of k as it results from relation (9), if one assumes that ε does not depend on k. This is generally untrue, but taking account of the dependence of ε on k would only introduce a slight quantitative modification of the graph of $E_0(k)$. The gaps for $k\in(-\pi,\pi)$ are intervals $(-k_1,0)$ and (k_2,π). The other fixed points (X_1,Y_1) of f are given by

$$X_1=\pm(\eta|E_0-2|)^{1/2},\quad Y_1=X_1$$

while the fixed points of $f^{(2)}(X_2,Y_2)$ are

$$X_2=\pm(\eta|E_0+2|)^{1/2},\quad Y_2=-X_2\ .$$

Figures 2(a) and 2(b) show the domains of existence of the

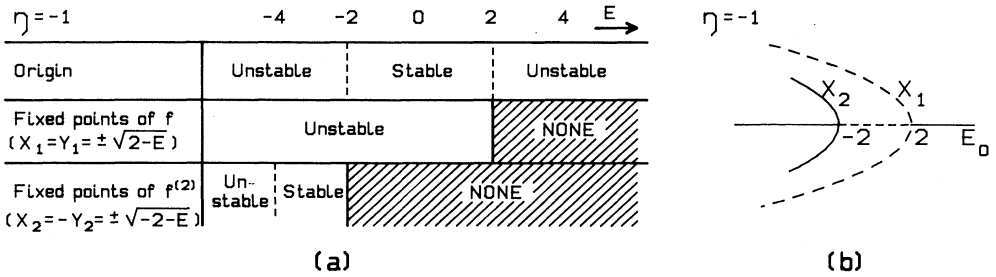

FIG. 2. (a) Table showing the domains of existence and the stability of the fixed points of f and $f^{(2)}$ for $\eta=-1$. (b) Bifurcation diagram of the fixed points.

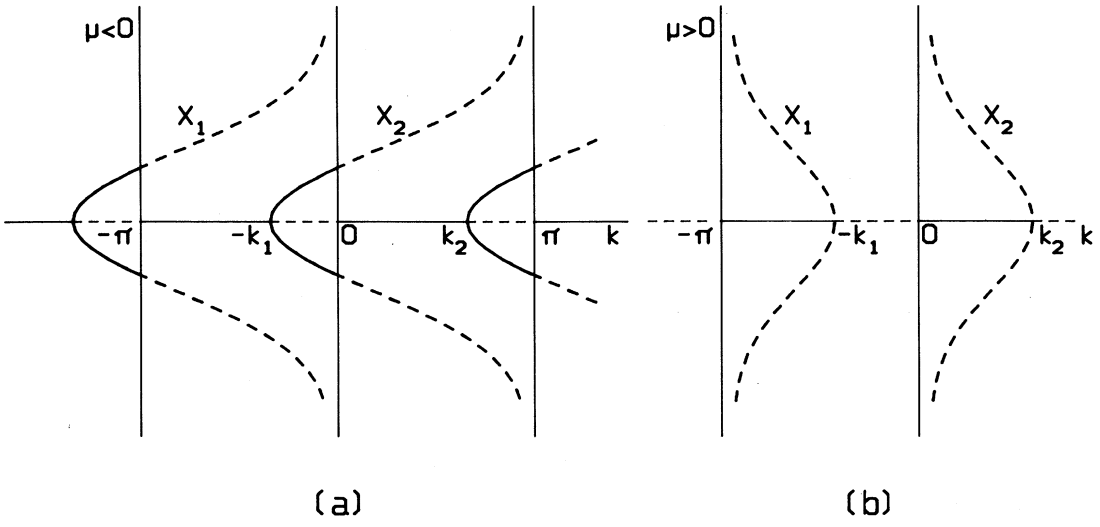

FIG. 3. Bifurcation diagrams in terms of parameter k: (a) for $\mu>0$, (b) for $\mu<0$.

fixed points and their stability in terms of E_0 for $\eta=-1$ together with the bifurcation diagrams of these fixed points. The bifurcation diagrams with respect to variable k are straightforwardly obtained from previous ones (in terms of E) thanks to relations (9) and (10). However, the transformation $\Psi_n \rightarrow \Phi_n$ is singular for $\sin k=0$ As a result, the fixed points of f and $f^{(2)}$ either remain at finite distance or go to infinity, depending on the sign of μ and of the k value ($k \simeq 0$ or $k \simeq \pi$). The resulting diagram is sketched in Fig. 3(a) for $\mu>0$ and Fig. 3(b) for $\mu<0$.

2. *Effect of the sign of the Kerr constant*

The bifurcation diagrams in terms of wave number k exhibit a strong dissymmetry between the cases $\mu>0$ and $\mu<0$. In particular we see that a system with positive Kerr constant has only hyperbolic fixed points (disregarding the origin). As we shall see below, this implies that such a system can support kink solutions but no solitonic ones, while the reverse is true in the case of a negative Kerr constant. This is a particular feature of our dicrete model. We shall show, in the study of the continuous model, that there always exist solitonic solutions inside the gaps, regardless of the sign of the Kerr constant.

C. Strong resonances and localized solutions

Consider an elliptic fixed point Ω of some iterate $f^{(k)}$ of the mapping. Its winding number ν is a continuous function of the control parameter (here E_0). Therefore it can take any rational value p/q. Then it appears (or "bifurcates") one or several period-q cycles with q elliptic points and q hyperbolic points. For $\nu=p/q+\lambda$ and in the case of a standard bifurcation, the distance of those points from Ω and the winding number of the elliptic points is of the order of $\sqrt{\lambda}$. There exist heteroclinic orbits connecting the hyperbolic points of the cycle which bound the domains of closed (or "quasiclosed") orbits around the elliptic points. Now the size of these domains shrinks to zero when $\lambda \rightarrow 0$ and the phase portrait around the origin is made of fairly regular closed orbits, except in a vanishingly small neighborhood of the cycle points. This fact is consistent with the KAM theorem which predicts the existence of analytic orbits inside an open neighborhood of the origin. Actually we shall later show how to calculate these orbits through an appropriate perturbative treatment.

However, there exist abnormal bifurcations which, although yielding analytic solutions in the neighborhood of the bifurcated point, modify qualitatively the orbits around Ω. These are the strong or Arnol'd resonances, and they appear at four values of the winding number, namely $\nu=1$, $\frac{1}{2}$, $\frac{1}{3}$, and $\frac{1}{4}$. Then the orbits around the bifurcated points are strongly modified with respect to regular KAM orbits, and , as a consequence, there appear observable localized solutions. The bifurcation parameter will be defined as

$$\varphi=2\pi\nu+\lambda \ .$$

1. *First and second resonances*

Consider first the bifurcations of the origin (and the case $\eta=-1$). The first resonance ($\nu=1, \varphi=2\pi$) appears when E_0 crosses value 2. From expression (11) the winding number of the origin is associated with $\lambda(|E_0-2|)^{1/2}$. For $E_0>2$ the origin is the only fixed point of f and it is unstable (see Fig. 2). For $E_0<2$ the origin becomes unstable (we are in the linear passing band), while there appears two hyperbolic fixed points on the first bissectrix, noted A_1 and B_1 in Fig. 4(a). The distance of these points to the origin goes to zero like λ, the orbits being more and more stretched along the bissectrix. A phase portrait of the kinklike solutions is shown in Fig. 4(a). Actually, for λ small but finite the solutions are not ana-

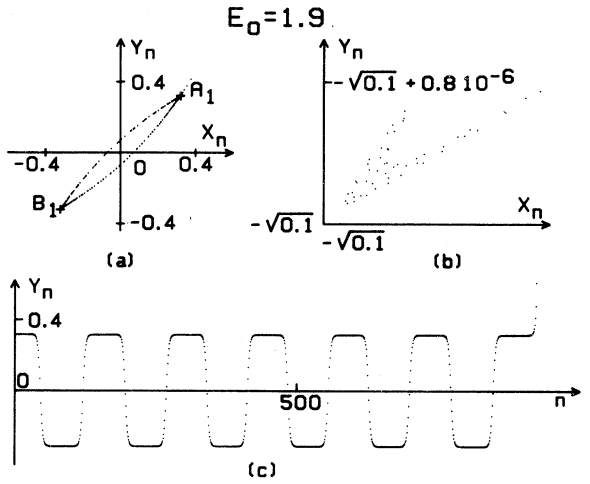

FIG. 4. (a) Phase portrait in the passing band near the gap edge. (b) Detail of the phase portrait near fixed point B_1. (c) Graph of $Y(n)$ showing the kink structure. At the end of the last plateau, the orbit diverges.

lytic. Figure 4(b) shows the details of an orbit in the vicinity of the origin (obtained by numerical iteration of the mapping), while Fig. 4(c) shows the spatial variation of such a solution.

We shall now show that, in the limit $\lambda \to 0$, the mapping becomes integrable inside a neighborhood of the origin including the fixed points. Let us set

$$x\sqrt{2}=\lambda u-\lambda^2 v \ ,$$

$$y\sqrt{2}=\lambda u+\lambda^2 v \ .$$

This new reference frame has its axis along the bissectrices, and the scaling of u and v by means of λ and λ^2 ensures that the hyperbolic fixed points remain at the same distance from the origin and the angle between the eigenvectors of these points is unchanged when $\lambda \to 0$.

The mapping reads, in terms of new variables u and v,

$$u'=(1-\lambda^2/2)u+\lambda(2-\lambda^2/2)v+(\lambda^2/4)(u+\lambda v)^3 \ , \tag{12}$$

$$v'=(1-\lambda^2/2)v-(\lambda/2)u+(\lambda/4)(u+\lambda v)^3 \ .$$

We see that $\Delta u=u'-u$ and $\Delta v=v'-v$ go uniformly to zero when $\lambda \to 0$, a fact which was expected since the winding number of the origin goes to zero. This suggests that the above mapping has integrable orbit solutions in this limit, and that these solutions are those of a continuous differential equation. Indeed we have

$$\frac{\Delta v}{\Delta u}=-(u+\lambda v)\frac{1-\frac{1}{2}(u+\lambda v)^2}{4v-\lambda(u+\lambda v)[1-\frac{1}{2}(u+\lambda v)^2]} \tag{13}$$

and we see that $\Delta v/\Delta u$ goes to a well-defined limit when $\lambda \to 0$. Then $\Delta v/\Delta u$ gets the meaning of the derivative dv/du, and Eq. (13) takes, in this limit, the form of the first-order differential equation:

$$\frac{dv}{du}=-\frac{u(1-\frac{1}{2}u^2)}{4v} \ . \tag{14}$$

This limiting procedure is justified because the solutions of Eq. (13) (where $\Delta v/\Delta u$ is replaced by dv/du) are continuous functions of λ, and converge towards the solutions of Eq. (14) when $\lambda \to 0$. These have the form

$$v^2=C+\frac{(1-\frac{1}{2}u^2)^2}{4} \ , \tag{15}$$

the separatrix (kink solution) corresponding to $C=0$.

The second strong resonance of the origin ($\nu=2, \varphi=\pi$) appears, for $\eta=-1$, when E_0 crosses value -2. For $E_0<-2$ the origin is unstable (linear gap). $f^{(2)}$ has two elliptic fixed points A_2, B_2 on the second bissectrix, and its distance to the origin is proportional to λ. Then one obtains orbits circling around A_2 or B_2, one of them being the homoclinic orbit of the origin [see Fig. 5(a)]. This type of solution is nothing but the so-called "gap solitons." Note that, considering the successive iterates of an orbit point by f instead of $f^{(2)}$, we should obtain points belonging alternately to the upper and lower plane. This means that the wave phase is reversed (or makes π jumps) on each successive modulation periods. Therefore we shall call these localized structures "alternate solitons."

A convenient way for obtaining the analytic solutions in the limit $\lambda \to 0$ [here $\lambda=(E_0+2)^{1/2}$] is to use symmetry property S, which amounts to consider mapping f (instead of $f^{(2)}$) with E_0 close to 2 and $\eta=1$. Note that, in this case, the solutions are now of the "nonalternate" type. The phase portraits of alternate solitons would be obtained from those of nonalternate solitons by simply

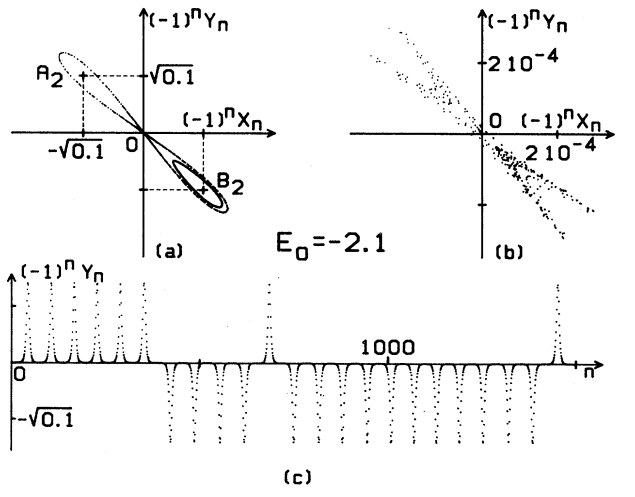

FIG. 5. (a),(b) Detailed phase portraits of solitonlike orbits showing the stochastic domains near the origin. (c) Graph of $(-1)^n Y(n)$. If the system were integrable all the peaks would have a positive sign. The stochasticity near the origin is responsible for the random sequence of peaks signs.

rotating the later phase portrait by $\pi/2$ around the origin. The calculation proceeds along the same lines as above, using the same scaling, and we obtain the following family of solutions:

$$v^2=C+\tfrac{1}{4}u^2(1-\tfrac{1}{4}u^2)\ , \tag{16}$$

the solitonic solution corresponding to $C=0$.

Figure 5 has the same meaning as Fig. (4) applied to the solitonic case. We shall comment later on the aspects related to the stochastic character of the solutions.

2. *Third and fourth resonance ($\nu=\frac{1}{3},\frac{1}{4}$)*

Their calculation is somewhat more complicated and it is convenient to call upon the standard treatment of normal forms (see, for instance, Arnol'd[5]).

A preliminary remark concerns the nonlinearities of the mapping. f exhibits only cubic nonlinear terms, a fact which rules out the possibility of the third resonance at the origin. We are therefore led to consider the more general problem of secondary bifurcations, namely the bifurcations of an elliptic fixed point P of $f^{(j)}$ instead of those of the origin.

Now it is convenient to project vector (X_n,Y_n) on the two eigenvectors of the mapping linearized around P. One obtains two components z_n,z_n^* which are complex conjugate, and z_{n+1},z_n,z_n^* obey the following recursion relation of the form:

$$z_{n+1}=e^{i\varphi}z_n+H(z_n,z_n^*)\ , \tag{17}$$

where

$$H=\sum_{k,p}a_{k,p}z_n^k(z_n^p)^*\ .$$

The calculation of the normal form consists, for given φ close to a rational value, and for small z_n, to make a change of variables of the form $z_n=\xi_n+\sum\alpha_{k,p}\xi^k(\xi^p)^*$, and to determine the $\alpha_{k,p}$'s in order to eliminate as many nonlinear terms as possible in Eq. (17). The set of irreducible (or nonremovable) terms constitutes the normal form. Relevant irreducible terms (i.e., with $k+p\leq 3$) are associated with the winding numbers $\nu=1,\ \frac{1}{2},\ \frac{1}{3},\ \frac{1}{4}$ (or $\varphi=2\pi\nu$). These winding numbers characterize the strong resonances.

The normal forms for $\nu=\frac{1}{3}$ and $\frac{1}{4}$ contain only two irreducible terms. They take the form

$$\xi_{n+1}=e^{i\varphi}\xi_n+i(A|\xi_n|^2\xi_n+Be^{i\varphi}(\xi_n^{j-1})^*$$

with $j=3,4$ and A and B being real coefficients. φ is close to $2\pi/j$.

Setting $\varphi=2\pi/j+\lambda(\lambda\ll 1)$, and $\xi_n=e^{i(2\pi n/j)}w_n$, we obtain that the w_n's obey the following recursion relation:

$$w_{n+1}=e^{i\lambda}w_n+i[A|w_n|^2w_n+B(w_n^{j-1})^*]\ .$$

In the limit $\lambda\to 0$ this relation yields a differential equation in terms of an arbitrary continuous variable t parametrizing the solution. It reads

$$dw/dt=i[\lambda w+A|w|^2w+B(w^{j-1})^*]\ . \tag{18}$$

In the case of a "normal bifurcation," $B=0$ and the solutions (18) correspond to elliptic orbits in the (X,Y) plane.

3. *Fourth resonance*

Being triggered by the cubic nonlinearity, the bifurcation of the period-4 cycle at the origin is a strong resonance. This resonance appears at a very low level of the wave energy, as do the first two resonances. It is observed for $\varphi\approx\pi/2$, or $E_0\approx 0$, that is, in the exact middle of the pass band. The coefficients of Eq. (18) here are $A=-\frac{3}{2}$ and $B=-\frac{1}{2}$ together with $j=4$.

Setting $\varphi=\pi/2+\lambda$ [with $\lambda=\sqrt{(-E_0)}$] and $w=\rho e^{i\theta}$, we obtain that ρ and θ obey the equations

$$d\rho/dt=(-\tfrac{1}{2})\rho^3\sin(4\theta)\ , \tag{19}$$

$$d\theta/dt=\lambda-(\tfrac{1}{2})\rho^2[3+\cos(4\theta)]\ . \tag{20}$$

The fixed points of these equations, which are also the fixed points of $f^{(4)}$, are such that $\theta=m\pi/4$ and $\rho^2(3+\cos 4\theta)=2\lambda$. Four of them are hyperbolic and are located in the (X,Y) plane on the middle of the sides of a square centered at the origin with side length $2\sqrt{(2\lambda)}$. We also have four elliptic points which are on the summits of this square [see Fig. 6(a)].

The following expression is an invariant of Eqs. (19) and (20):

$$K=4\lambda\rho^2-[3+4\cos(4\theta)]\rho^4\ . \tag{21}$$

Remembering that $X=2\rho\cos\theta$, $Y=-2\rho\sin\theta$, Eq. (21) is a polar representation of the family of continuous orbit solutions in the neighborhood of the origin. $K=\lambda^2$ corresponds to the curves containing the hyperbolic points (heteroclinic orbits). Their equations, in terms of X,Y variables, are

$$X^2+Y^2\pm\sqrt{2}XY=2\lambda \tag{22}$$

and they represent two ellipses centered at the origin and whose axes are the bissectrices. They are entangled into each other, forming a cross [see Fig. 6(a)]. These ellipses become λ independent through the variable change $X\to X\sqrt{\lambda}, Y\to Y\sqrt{\lambda}$, which shows that their shape is preserved when $\lambda\to 0$. In particular, the area of the domains of closed orbits around the elliptic points ("elliptical domains") remains a finite fraction α of the ellipses' area. On the contrary, $\alpha\to 0$ when $\lambda\to 0$ in the case of a weak resonance. The orbit by $f^{(4)}$ of a point in such a domain containing elliptic point P lies on a closed curve surrounding P. Therefore, iterates $Y^{(4)}(n)$ of $f^{(4)}$ exhibit a spatial variation which is periodic around a nonzero average value (corresponding to the coordinates of the elliptic point contained in the chosen elliptical domain).

For $E_0=-0.1$, Fig. 6(b) shows the graph of $Y^{(4)}(n)$ associated with the orbit of a point very close to a hyperbolic point. One observes three plateaus corresponding to amplitudes 0, $\pm\sqrt{(2\lambda)}$. The sequence of these three plateaus and of the peaks which precede or follow them is obviously random. We shall come back later to this point. Figure 6(c) shows $Y^{(4)}(n)$ associated with an orbit

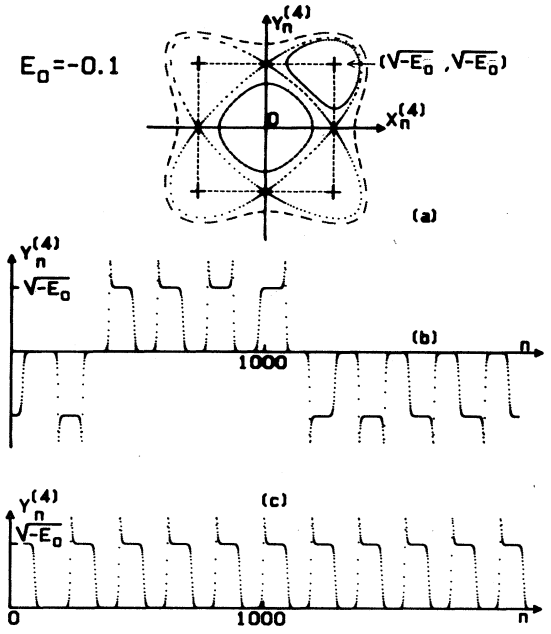

FIG. 6. (a) Phase portrait of a period-4 cycle for $\lambda=\sqrt{0.1}$. (b) Graph of $Y^{(4)}(n)$ corresponding to the orbit of a point very close to one of the cycle hyperbolic points. One notes the random sequence of three plateaus preceded or followed by sharp peaks. These peaks are associated with rapid turns around the cycle elliptic points.

located inside an elliptical domain (but still close to a heteroclinic orbit). One observes an anharmonic oscillation around a nonzero average value. These features are characteristic of a new localized structure which we call "square." Note that, in the case of a normal bifurcation and in the limit of small λ, elliptical domains would be unaccessible.

4. *Third resonance*

The bifurcation of a period-3 cycle at the origin is not resonant because of the absence of quadratic nonlinearity in mapping f. We shall therefore consider a secondary bifurcation. The simplest one is the bifurcation of an elliptic point P of f inside a gap (case $E_0>2$, $\eta=1$). Remember that this point was issued from the bifurcation of the origin at $E_0=2$. It is located on the first bissectrix at the distance $\xi=(E_0-2)^{1/2}$ from the origin, and its winding number is $\nu=\varphi(2\pi)$ with $\cos\varphi=3-E_0$. For $\varphi=2\pi/3$, $E_0=\frac{7}{2}$ and ξ takes the finite value $\sqrt{\frac{3}{2}}$. Therefore the third resonance cannot be observed for small wave amplitude. This conclusion holds regardless of the chosen bifurcated elliptic point. In the present case the above value of E_0 corresponds to $\varepsilon>1$, a somewhat unphysical situation. But this resonance can also be observed for small ε inside a passing band, by considering the bifurcation of any elliptic point belonging to a cycle with period equal or larger than 3. The phenomenon would be quite analogous (same kind of normal form). Let us therefore analyze the simpler case above (i.e., the bifurcation of an elliptic point P of f). Putting

$$X=\xi+x, \quad Y=\xi+y ,$$

the mapping equations take the form

$$x'=y ,$$

$$y'=-x+2(3-E_0)y-3\xi y^2-y^3 ,$$

and the associated normal form for $\varphi=2\pi/3+\lambda$ is Eq. (18) with $\lambda=(2/\sqrt{3})(E_0-\frac{7}{2})$, $A=\sqrt{3}$, and $j=3$.

In the limit $\lambda\to 0$ the cubic term can be neglected in Eq. (18). This equation then yields three fixed hyperbolic points in the (X,Y) plane whose coordinates in a reference frame centered in P are (ρ,ρ), $(\rho,-2\rho)$, $(-2\rho,\rho)$, with $\rho=\lambda\sqrt{2/3}$. These points are the summits of a rectangle isoceles triangle (see Fig. 7). Several remarks are in order.

(a) The previous bifurcations were one sided (or of the pitchfork type). Indeed the coordinates of the bifurcated fixed points were expressed in terms of $\sqrt{\lambda}$, and λ must be positive. Here, on the contrary, the bifurcated state exists on both sides of the bifurcation value (λ positive or negative), the bifurcated solutions being symmetrical versus elliptic point P when λ is changed to $-\lambda$.

(b) The distance of these points from P is of the order of λ instead of $\sqrt{\lambda}$ in the case of the fourth resonance. This shows that the domain of KAM regular orbits around P is smaller for the same deviation λ from the resonant winding number.

(c) There exists other fixed points, elliptic and hyperbolic of $f^{(3)}$. But they are found at finite distance from P (and cannot be obtained through the perturbative treatment).

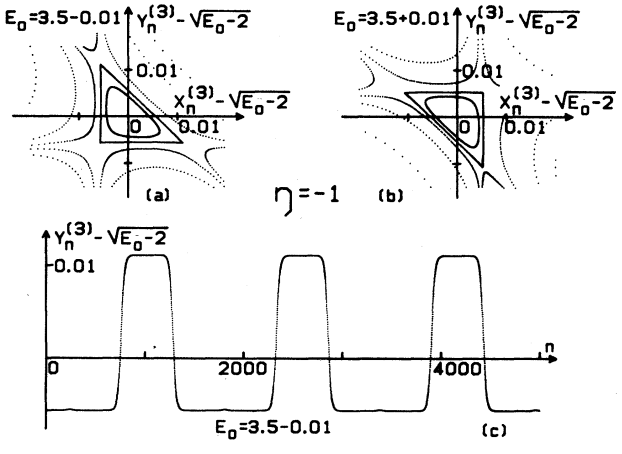

FIG. 7. Bifurcation of an elliptic point P of f inside a gap, giving rise to a period-3 cycle (strong resonance). (a) Phase portrait of $f^{(3)}$ in the neighborhood of P for $\lambda=-0.01$. (b) Same phase portrait for $\lambda=0.01$. The bifurcation is double sided, and the domain of regular orbits around P is bounded by an isoceles rectangle triangle. (c) The graph of $Y^{(3)}(n)$ corresponding to a heteroclinic orbit exhibits two plateaus.

(d) Equation (18), without the cubic term, yields the following differential equations obeyed by real variable x and y:

$$\sqrt{3}\,dx/dt=(x+2y)[\lambda-(3/\sqrt{2})x]\ ,$$

$$\sqrt{3}\,dy/dt=-(y+2x)[\lambda-(3/\sqrt{2})y]\ .$$

These equations show that the heteroclinic orbits joining the three fixed points are nothing but the sides of the above rectangle triangle. Obviously the shape of this triangle is preserved when $\lambda\to 0$.

(e) The orbits are quite regular inside the triangle, but apparently chaotic outside, except in a small neighborhood of three elliptic points of $f^{(3)}$ located very far from the triangle.

The above features are characteristic of the new localized structure which we call "triangle." These structures are only obtained for finite wave amplitude.

D. Stochastic behavior of the localized solutions

Determining the measure of the stochastic domains in a mapping of the plane into itself is still an open problem. We only remark, according to numerical results, that strong resonances obviously play a major role. Indeed, as soon as a resonant cycle is created, important nonlinear effects appear in the neighborhood of the bifurcated point. We have already observed stochastic domains near the hyperbolic points of the various localized structures even near the bifurcation value.

Now we know that the system becomes integrable in the neighborhood of the bifurcated point. However, some residual stochasticity survives near the hyperbolic points of the cycle, and it manifests itself by two major physical effects.

(i) Perfect localization is impossible. We mean that one cannot find in a large system a stationary solution in which a characteristic variable (amplitude or phase of the wave) exhibits a rapid variation around only one space point ("one-peak solution"). Perfect localization is characteristic of an integrable system in which an orbit can approach a hyperbolic point as close as is wanted. But this is practically impossible in a nonintegrable system, due to the shape of the stable and unstable manifolds of the hyperbolic points. As a result, there exists a maximum spatial extent (or MSE) of a localized solution. In the solitonic case the solutions will generically exhibit multipeaks. The same phenomenon appears in the kink case (outside the linear gap), but the sequence of peaks is necessarily limited because bounded and divergent orbits are "connected" near the hyperbolic points.

(ii) The stochasticity manifests itself by sudden π variations of the wave phase, and this occurs in a random way. Let us for instance consider a nonalternate soliton. Its orbit in the (X,Y) plane would stay in the same half plane if the system were integrable. Actually the orbits in the two half planes are "connected" near the origin. Passing from one half plane to the other one means that the wave phase exhibits a π variation. The orbit makes a random successive number of turns around each elliptic point. The same phenomenon is expected in the case of an alternate soliton, by observing the phase one time out of two periods (orbit of $f^{(2)}$). Figure 5 shows this stochastic behavior.

Stochasticity produces random variations of the field amplitude in the case of the fourth resonance. The interpretation of Fig. 6(b) is the following. When an orbit reaches the neighborhood of a hyperbolic point P of the cycle, two elliptical paths are available: the shortest connects P to the nearest hyperbolic point in an anticlockwise sense; the second connects P to the other nearest neighbor in the clockwise sense, by circling around the neighboring elliptic point. This explains the randomness of the plateaus sequence and also the peaks of the figure: they are associated with the rapid turns around the elliptic points.

We now want to analyze the first effect in more detail, and show numerically that the onset of stochasticity near the bifurcation of a resonant cycle looks like a critical phenomenon, characterized by a critical exponent. Let us consider the kink case. In the integrable limit ($\lambda\to 0$), the bounded orbits (located inside the separatrice) are symmetrical with respect to the origin. The stochasticity will break this symmetry, and we propose to study this effect in the following way. We consider the orbits of initial points M located on the bissectrix at a variable distance δ from one of the hyperbolic fixed points, say A_1 (see Fig. 8). For large enough δ, M belongs to a regular orbit accurately described by Eq. (15). Then, if δ' is the shortest distance of an orbit point from the second hyperbolic fixed point B_1 (along the first way from A_1 to B_1), we have $\delta'\approx\delta$. Decreasing δ, the graph of δ' as a function of δ is horizontal up to a definite value δ_c where it exhibits a sharp transition from a constant value to a chaotic regime (see Fig. 9).

δ_c corresponds to a number N_c of mapping iterations ($\delta_c\gamma^{N_c}\simeq\sqrt{\varepsilon}$, γ being the Floquet exponent of the hyperbolic point which is larger than unity). N_c is about the maximum number of iterations needed for going from A_1 to B_1 without escaping afterwards to infinity or going back to A_1. In other words, N_c is a measure of the above-mentioned MSE. The variation of N_c is a function

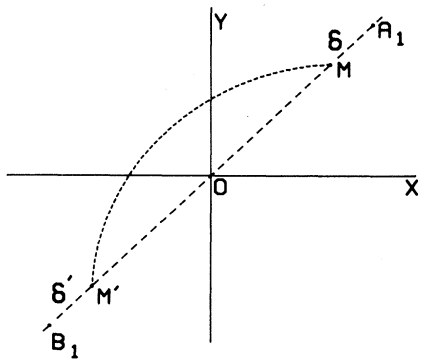

FIG. 8. Geometry of a kinklike orbit with distances δ and δ' defined in the main text.

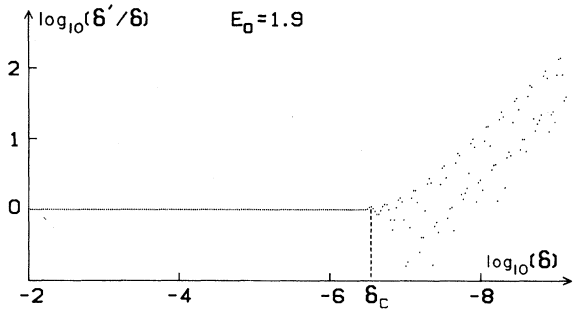

FIG. 9. Sharp boundary of the stochastic domain around a hyperbolic point. Graph of δ' as function of δ.

of λ whose graph is shown in Fig. 10.

We observe that this graph exhibits a set of nearly horizontal plateaus connected by sharp discontinuities, the plateau widths decreasing when $\lambda \to 0$. It appears that the discontinuities take place for $\lambda = \lambda_m$ with λ_m close to $2\pi/m$ (m integer). For such a λ value a period-m cycle with winding number $1/m$, which may be called a "primary cycle," bifurcates at the origin. Actually λ_m is found to be slightly different from $2\pi/m$, and equal to the winding number of the m primary cycle, one point of which is distant from A_1 by δ_c. In other words, $1/m$ is the winding number of the last primary cycle encountered before entering the "stochastic domain." This result indicates the importance of primary cycles in the overall stochastic behavior of the solutions. The graph $N_c(\lambda)$ is increasingly close to a continuous curve as λ approaches zero. This limit function $N_c(\lambda)$ is very well fitted by a power law: $N_c \simeq \lambda^{-\nu}$ with $\nu \approx 1.4$. ν is the critical exponent characterizing the onset of stochasticity on the left side of the gap edge.

The same type of calculation performed in the soliton case yields the same critical exponent ν ($N_c \simeq \lambda'^{-\nu}$). In this case, N_c is the maximum spatial extent of a pseudo-soliton. For $N > N_c$ we get the multipeaked solutions shown in Fig. 7(c).

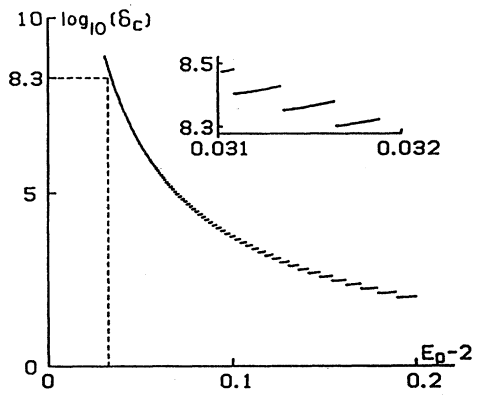

FIG. 10. Graph of $\log_{10}(\delta_c)$ (or N_c) as a function of $\lambda^2 = E_0 - 2$. It is made of a set of plateaus whose width is a decreasing function of λ. For small λ we find that the variation of N_c is well fitted by $N_c \simeq \lambda^{\nu}$ with $\nu = 1.4$.

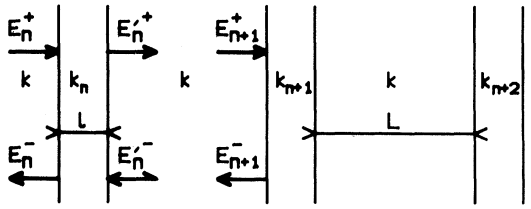

FIG. 11. Inward and outward fields around a barrier.

ACKNOWLEDGMENTS

The authors are grateful to Dr. P. Coullet for important comments about Arnol'd resonances.

APPENDIX: THE DISCRETE MODEL

In this model we have a set of thin equidistant dielectric sheath with a nonlinear refractive index. They are represented in Fig. 11, together with the fields $E_j^{\pm}$ propagating, respectively, towards the right side and the left side. k_j is the refractive index of the jth sheath.

Writing the continuity of the $E^{\pm}$ fields and of their derivatives through the boundaries of the nth sheath, we obtain

$$\begin{bmatrix} E_n'^{+} \\ E_n'^{-} \end{bmatrix} = \begin{bmatrix} \alpha_n & \beta_n \\ \beta_n^* & \alpha_n^* \end{bmatrix} \begin{bmatrix} E_n^{+} \\ E_n^{-} \end{bmatrix},$$

where

$$\alpha_n = (1/4\rho_n)[(\rho_n+1)^2 e^{i\varphi_n} - (\rho_n - 1)^2 e^{-i\varphi_n}],$$

$$\beta_n = (i/2\rho_n)(\rho_n^2 - 1)\sin\varphi_n,$$

with

$$\rho_n = k_n/k, \quad \varphi_n = k_n l .$$

In the limit $l \to 0$, $k_n/k \to \infty$, and $k_n^2 l/k \to 2\varepsilon_n$, α_n and β_n read

$$\alpha_n = 1 + i\varepsilon_n, \quad \beta_n = i\varepsilon_n .$$

ε_n will be taken of the form $\varepsilon_n = \varepsilon(1 + \mu|\Psi_n|^2)$.

Now we easily obtain the matrix relation between fields $E_n^{\pm}$ and $E_{n+1}^{\pm}$, which reads

$$\begin{bmatrix} E_{n+1}^{+} \\ E_{n+1}^{-} \end{bmatrix} = \begin{bmatrix} a_n & b_n \\ a_n^* & b_n^* \end{bmatrix} \begin{bmatrix} E_n^{+} \\ E_n^{i} \end{bmatrix}$$

with

$$a_n = (1 + i\varepsilon_n)e^{ik},$$

$$b_n = i\varepsilon_n e^{ik},$$

where we have assumed sheath separation L equal to unity. From the above matrix relation, we deduce that $\Psi_n = E_n^{+} + E_n^{\mp}$ obeys recursion relations (4) and (5) of the main text.

[1]F. Delyon, Y. Levy, and B. Souillard, Phys. Rev. Lett. **57**, 2010 (1986).
[2]D. Mills and S. Trullinger, Phys. Rev. B **36**, 947 (1987).
[3]Mira Gumowski, *Dynamique Chaotique* (Cepadues, 1980), p. 285.
[4]P. Bak, V. Pokrovsky Phys. Rev. Lett. **47**, 958 (1981).
[5]V. Arnol'd, *Supplementary Chapters of the Theory of Ordinary Differential Equations* (Mir, Moscow, 1978), Chap. 5.